

Westinghouse MAO
MER-98-2

MAO-T--98-0233
MER--98-2
CONF-980657--

Ductility Dip Cracking Susceptibility of Inconel Filler Metal 52 and Inconel Alloy 690

Jeffrey M. Kikel, BWX Technologies, Inc.

David M. Parker, Westinghouse Electric Company

Abstract:

Alloy 690 and Filler Metal 52 have become the materials of choice for commercial nuclear steam generator applications in recent years. Filler Metal 52 exhibits improved resistance to weld solidification and weld-metal liquation cracking as compared to other nickel-based filler metals⁽¹⁾. However, recently published work indicates that Filler Metal 52 is susceptible to ductility dip cracking (DDC) in highly restrained applications⁽²⁾. Susceptibility to fusion zone DDC was evaluated using the transverse vareststraint test method, while heat affected zone (HAZ) DDC susceptibility was evaluated using a newly developed spot-on-spot vareststraint test method. Alloy 690 and Filler Metal 52 cracking susceptibility was compared to the DDC susceptibility of Alloy 600, Filler Metal 82, and Filler Metal 625. In addition, the effect of grain size and orientation on cracking susceptibility was also included in this study.

Alloy 690, Filler Metal 82, Filler Metal 52, and Filler Metal 625 were found more susceptible to fusion zone DDC than Alloy 600. Filler Metal 52 and Alloy 690 were found more susceptible to HAZ DDC when compared to wrought Alloy 600, Filler Metal 82 and Filler Metal 625. Filler Metal 52 exhibited the greatest susceptibility to HAZ DDC of all the weld metals evaluated. The base materials were found much more resistant to HAZ DDC in the wrought condition than when autogenously welded. A smaller grain size was found to offer greater resistance to DDC. For weld metal where grain size is difficult to control, a change in grain orientation was found to improve resistance to DDC.

Introduction:

DDC was observed in highly restrained Filler Metal 52 welds. The cracking was along grain boundaries and up to 0.120" in length and 0.040" in depth. These cracks typically occurred in the heat affected zone (HAZ) of previously deposited weld metal; although some may have occurred in the fusion zone after solidification. HAZ DDC was observed to occur at some distance (approximately 0.12 inch) from the fusion line. This distance correlates with a temperature range well below liquation cracking temperatures.

DDC is an elevated temperature solid-state form of cracking, which occurs intergranularly during weld cooling due to a sharp loss in material ductility. DDC typically occurs in materials, which have an austenitic (fcc) crystal structure and would otherwise be expected to exhibit ductile behavior. Figure 1 is a schematic illustration of ductility as a function of temperature and shows ductility dip behavior. The drop in ductility occurs at a temperature in the vicinity of the recrystallization temperature⁽³⁾. If the thermal strains from fabrication intercept the dip in ductility, cracking occurs.

It has been shown that in weld metal, DDC occurs preferentially along migrated grain boundaries⁽⁴⁾. Single phase weld metals with low amounts of grain boundary precipitates and/or second phases have little resistance to grain boundary movement and hence had a higher prevalence of migrated boundaries and a greater tendency for DDC. Materials that have low impurity levels with low grain boundary precipitates and/or second phases would have little resistance to grain boundary movement and should be more susceptible to DDC. The alloys in this study are all low in impurities, and only FM 82 and FM 625 have a grain boundary second phase – a niobium carbide eutectic.

These efforts were undertaken to establish a methodology to permit order ranking of DDC susceptibility for various materials and to provide a screening method for replacement material selection. Previous studies with both single spot and longitudinal vareststraint testing revealed DDC but were not effective in quantifying DDC susceptibility due to random orientation of the grain boundaries. It was

DISCLAIMER

This report was prepared as an account of work sponsored by an agency of the United States Government. Neither the United States Government nor any agency thereof, nor any of their employees, makes any warranty, express or implied, or assumes any legal liability or responsibility for the accuracy, completeness, or usefulness of any information, apparatus, product, or process disclosed, or represents that its use would not infringe privately owned rights. Reference herein to any specific commercial product, process, or service by trade name, trademark, manufacturer, or otherwise does not necessarily constitute or imply its endorsement, recommendation, or favoring by the United States Government or any agency thereof. The views and opinions of authors expressed herein do not necessarily state or reflect those of the United States Government or any agency thereof.

DISCLAIMER

**Portions of this document may be illegible
electronic image products. Images are
produced from the best available original
document.**

apparent that grain boundary orientation relative to the applied strain had a significant effect on the test results and repeatability. Since the cracking is predominant on long grain boundaries, it was theorized that fusion zone DDC would be more apparent with transverse vareststraint testing. The centerline of the test weld in transverse vareststraint testing is perpendicular to the applied strain. For HAZ DDC it was thought that the use of a large pre-spot for preferential grain orientation, radially outward from the test spot, would provide the best orientation of the grain boundaries to the applied strain.

Experimental Procedure:

Five materials were tested: Filler Metal 52 (FM 52), Filler Metal 82 (FM 82), Filler Metal 625 (FM 625), Alloy 690, and Alloy 600. The filler metals were deposited in pads by hot wire gas tungsten arc welding shielded with argon. The weld pads were 0.75 inch minimum height. The filler metal specimens were removed parallel to the top surface of weld pads. For the pre-spot vareststraint testing, a second set of FM 82 specimens were removed perpendicular to the weld pad top surface. The base metal specimens were machined from wrought plate. The test metal compositions are in Table 1. The specimens were 0.25 inch thick and bent over a radiused block following the Edison Welding Institute developed vareststraint testing methodology. Figure 2 shows a schematic of the transverse vareststraint and spot vareststraint testing configuration.

The transverse vareststraint tests were conducted at augmented strain levels of 4, 5, and 7% – all with a constant bend rate of 10 inches per second (ips). Additionally, constant strain tests were conducted at variable bending rates. The test conditions are listed in Table 2. The total crack length, number of cracks, cracking location, cracking temperature range, threshold strain, and threshold bend rate were determined. Three tests were run for each test condition.

The spot vareststraint tests were conducted on as-received specimens and specimens with pre-spot welds. The pre-spot welds provided preferentially oriented microstructure, which would minimize variability

from specimen to specimen. The pre-spot weld was made on the test plate with gas tungsten arc welding. Then a second, smaller spot weld was made, the arc was extinguished, and after a 0.5 second delay the plate was bent over the radiused block. The test conditions are listed in Table 2. Figure 3 is an illustration showing a plan view of the spot-on-spot test showing the DDC cracking region. Augmented strain levels of 5, 7, and 10 % were run with a constant bend rate of 10 ips. Temperature profiles were obtained by the plunged thermocouple technique. Additionally, threshold strain tests were conducted. The number of cracks, crack location, and cracking temperature range were determined. Slow bend rate tests were conducted with FM 82 and Alloy 690 spot-on-spot specimens at a constant strain of 7% and bend rates of 1 and 2.5 ips. The slow bend rate tests were performed to compare fractography on DDC cracks generated using strain rates more typical of actual welding. The cracks were measured with up to 40X light microscopy.

Conventional metallography and fractography was also performed.

Results:

The transverse vareststraint testing results are shown in Table 3. The ductility dip cracks typically started 0.118 inch (3 mm) from the fusion line of the molten weld pool at the time of bending and extended to 0.315 to 0.394 inch (8 to 10 mm). The corresponding temperature ranges for DDC were 1200°C to 941°C. Figure 4 shows DDC observed in a typical as-tested transverse vareststraint sample. As can be seen in this figure, DDC does occur a significant distance from the solid/liquid interface. During transverse vareststraint testing, Alloy 600 did not exhibit any fusion zone DDC. Alloy 690 exhibited a DDC threshold strain of less than 4% and a threshold bending rate of .04 ips, which was similar to that of FM 82 and FM 52. FM 625 had a threshold strain of 5% with a 2 ips threshold bending rate for the occurrence of DDC although extensive liquation cracking was noted. From the total number of ductility dip cracks, the greatest resistance to fusion zone DDC was exhibited by Alloy 600 which had no cracking, followed by FM 625, FM 52 and FM 82, and, lastly, Alloy 690. Comparison of total crack length, crack location, and the corresponding

cracking temperature range yielded no clear separation between Alloy 690, FM 52 and FM 82 in susceptibility to fusion zone DDC. This was contradictory to weld mock-ups where FM 52 weld exhibited extensive DDC and FM 82 welds had very limited cracking in both length and occurrence.

Grain boundary orientation relative to the direction of the applied strain is a primary factor in forming DDC. The orientation of grain boundaries in the autogenous transverse vareststraint test beads varied in direction from 10 to 50 degrees from the applied strain. This would produce considerable differences in local strains across the grain boundaries. Variability of the grain boundary orientation between samples and between each material was significant, resulting in the inability to clearly separate and rank the fusion zone DDC susceptibility of each material.

The grain boundary orientation variability observed during transverse vareststraint testing led to the concept of preconditioning the vareststraint test specimens to achieve similar grain boundary orientations in all samples. It was anticipated that more consistent results and a more direct comparison between materials would be achieved for HAZ DDC if all samples had similar grain orientations. A spot gas tungsten arc weld was selected for this preconditioning of vareststraint specimens in conjunction with the spot vareststraint test. Figure 5 shows a plan view micrograph of a typical pre-spot weld on a test sample. Figure 6 shows a comparison of the initial FM 52 weld deposit microstructure to the microstructure of the FM 52 pre-spot. As can be seen in this figure, the pre-spot produced long grain boundaries radially oriented outward from the center. This grain orientation did maximize HAZ DDC during testing. The increase in grain size with the pre-spot can be seen by comparing the as-deposited samples to samples tested using the pre-spot. Figure 7 depicts the tremendous increase in grain size from the wrought Alloy 600 and Alloy 690 to the pre-spot condition of Alloy 600 and Alloy 690. Also obvious in Figure 7 is the much smaller grain size of the wrought Alloy 600 when compared to the wrought Alloy 690.

The number of cracks, crack location, threshold strain, and cracking temperature range for the spot-on-spot vareststraint testing is shown in Table 4. FM 625 results are not reported due to the extensive liquation

cracking observed during testing. Although the ductility dip crack could be readily distinguished from the liquation cracks, the liquation cracking appeared too extensive to consider FM 625 as a viable replacement filler metal in highly restrained applications. The crack locations were converted to temperature values using temperature profiles obtained by plunging a Type C, tungsten-rhenium thermocouple into the molten weld puddle of sample spot welds. The cracking locations were based on the fusion boundary of the test spot being defined as the zero coordinate. Cracking that extended into the test spot was given a negative number, while cracking in the pre-spot was given a positive number. Figure 8 shows a typical example of DDC in an as-tested spot-on-spot vareststraint test.

Figure 9 is a graphical representation of the DDC temperature range for each material along with the corresponding threshold strain. A larger DDC temperature range is indicative of a wider dip in ductility and an increase in DDC susceptibility. A lower threshold strain represents a lower ductility and an increase in DDC susceptibility. The spot-on-spot testing produced large cracking temperature ranges, which were much greater than those in the transverse vareststraint testing. It is apparent from the crack temperature ranges that Alloy 690 without a pre-spot is more susceptible to HAZ DDC than Alloy 600 without a pre-spot, and that Alloy 690 with a pre-spot is more susceptible than Alloy 600 with a pre-spot. Further, FM 52 is much more susceptible to HAZ DDC than FM 82. It is also apparent that pre-spot conditioning dramatically increases the extent of HAZ DDC. Figure 9 shows the similarity in HAZ DDC temperature ranges of FM 82 with a pre-spot and the FM 82 sample removed at 90° to the weld pad surface. The use of the pre-spot conditioning also reduces the threshold strain for HAZ DDC from 10% to 3% for Alloy 600, from 3% to 1% for Alloy 690, and from 3% to 2% for FM 82.

Using the threshold strain and the cracking temperature limits, DDC envelopes can be created. The threshold strain (minimum augmented strain to initiate DDC) forms the bottom of the DDC envelope, and the cracking temperature limits form the sides. Figure 10 shows the DDC envelope for Alloy 690 and Alloy 600 with and without the pre-spot, with the Alloy 690 pre-spot exhibiting about a 175°C drop in the lower

bound for DDC when compared to the wrought Alloy 690. The Alloy 600 lower bound drop with the pre-spot was estimated at 300°C. The use of the pre-spot results in a significant increase in the DDC envelope for Alloy 690 and Alloy 600. Figure 11 shows the DDC envelope for FM 52 and FM 82 with the pre-spot and FM 82 without the pre-spot. The effect of the pre-spot in increasing the DDC envelope for FM 82, 75°C shift in lower bound, can be seen in Figure 11 as well as the difference between the FM 52 and FM 82 DDC lower bound of 150°C. In each material the use of the pre-spot increased the DDC envelope -- reducing the materials resistance to DDC. In the pre-spot condition, some grain boundaries are always oriented to the maximum strain. Additionally, the large grain size in the pre-spot provides fewer boundaries to distribute this stress resulting in greater strain localization at each boundary. The pre-spot produces a condition similar to actual weld buildups; e.g. the FM 82 samples removed at a 90° orientation from the deposited weld pads and tested without a pre-spot. The DDC temperature limits of the weld are very similar to those of the FM 82 test samples with pre-spots. In the FM 82 samples removed parallel to the weld pad upper surface, grain growth ran through the .250" thickness of the sample. Since the face was perpendicular to the grain growth, grain size appears small as shown in Figure 6a. The samples removed 90 degrees to the weld pad upper surface had grain growth perpendicular to the .250" thickness of the sample as shown in Figure 6b. Since the face of the sample was running parallel with the grain growth, grains were large and elongated, typically of a weld build-up.

Based on the spot-on-spot vareststraint testing results, combining the threshold strain and the DDC temperature limits, Alloy 690 with the pre-spot was found to be the most susceptible material to DDC. The second most susceptible material to DDC is FM 52. Alloy 600 and FM 82 with pre-spot, wrought Alloy 690, and 90° orientation Filler Metal 82 had similar susceptibility to DDC. Alloy 600 without the pre-spot was clearly the least susceptible to DDC, followed by FM 82 without the pre-spot. Slow bend rate testing of FM 82 and Alloy 690 samples with pre-spots also showed a difference in DDC susceptibility. Bending rates of 1 and 2.5 inches per second, to simulate actual welding strains, produced no cracking in FM 82, while

cracking was observed at 1 inch per second in Alloy 690. No cracks were observed at 2.5 inches per second in the Alloy 690 bend sample.

Fractography revealed smooth-intergranular to ductile-intergranular fracture. Comparison of the high temperature crack surface to the low temperature end showed little difference in the most susceptible materials when using a fast bend rate of 10 inches per second. Figure 12 shows the fracture surface of the low and high temperature ends of a DDC in FM 52 with pre-spot. Figure 13 shows the fracture surface of the low and high temperature ends of a DDC in Alloy 690 with pre-spot. A slow bend rate crack fracture surface from the Alloy 690 spot-on-spot sample, Figure 14, was found to transition from a liquation type crack to a solid state ductility dip crack with smooth intergranular features.

Discussion:

Both fusion zone and heat affected zone DDC were observed in this. DDC did occur in all the weld and base metals tested in this study, although there was no fusion zone DDC produced in Alloy 600. In this study the augmented strain from the vareststraint test represented the weld stresses of a highly restrained application and triggered the occurrence of DDC. The transverse vareststraint testing with the number of cracks, threshold strain and threshold strain rate did clearly show no susceptibility of Alloy 600 to fusion zone DDC and the high susceptibility of Alloy 690. The high susceptibility of Alloy 690 would suggest Alloy 690 would have a poor performance in autogenous welding. As pointed out earlier, the variability in grain orientation to applied strain would contribute to the inability to separate FM 52 from FM 82. It could be presumed that FM 52 and FM 82 are equal in their susceptibility to fusion zone DDC and that the DDC observed in actual welds was HAZ DDC. It is also noted that the transverse vareststraint DDC temperature ranges were smaller than those determined in the spot-on-spot vareststraint tests. This smaller temperature range is attributed to the angle of the grain boundaries varying 10 to 50° from the applied strain.

In reviewing the results of the spot-on-spot vareststraint tests, large grain size and orientation have a major influence on increasing DDC susceptibility. Increasing grain size causing increased susceptibility to

DDC would be similar to the grain size effect seen in other types of grain boundary cracking phenomena. As grain size increases the amount of grain boundary area decreases. For DDC, as the grain boundary area decreases, the local strains at the remaining grain boundaries increase to the point of rupture. Comparison of the test results with Alloy 600 and Alloy 690 in the wrought and then pre-spot conditions dramatically demonstrates the effect of grain size on HAZ DDC with a shift of 175°C or greater in the lower temperature bound of the DDC envelope. The grain size of the least susceptible material, wrought Alloy 600, was at least half that of wrought Alloy 690. This grain size difference is a large contributor for the difference in DDC susceptibility between Alloy 600 and Alloy 690. The DDC in Alloy 600 and Alloy 690 with pre-spots would represent cracking of an autogenous weld after a subsequent weld pass was deposited. From the DDC envelopes of Figures 10 and 11, the DDC low temperature bound and the threshold strain were the most instrumental parameters in showing the effects of grain size on HAZ DDC and permitting separation of the materials tested for ranking to HAZ DDC susceptibility.

The large grain size contribution to HAZ DDC susceptibility is also apparent in FM 82 tests where the pre-spot conditioning shifted the DDC envelope lower temperature bound by 75°C and reduced the threshold strain for DDC from 3% to 2%. The FM 52 and FM 82 with pre-spot welds simulates production weld build-up, and the vareststraint augmented strain represents strain imposed in the through thickness of the build-ups by welding a subsequent joint; e.g. a safe end closure weld. Reduced DDC susceptibility could be attained by ensuring a more resistant grain orientation -- in the weld safe end, the weld grain orientation should be radial.

The 150°C lower temperature bound difference in Figure 11 between FM 52 and FM 82, both with pre-spots could be explained by composition. Materials containing grain boundary second phases like a eutectic constituent would have a greater resistance to grain boundary migration and would have limited grain growth at elevated temperatures. The resistance to grain boundary migration and restriction of grain growth is the result of the eutectic pinning grain boundaries at elevated temperatures. Materials without the secondary

phases on grain boundaries, Alloy 690 and FM 52, had large grains with long straight grain boundaries and were the most susceptible to DDC.

Due to similar appearance during optical metallography, it is difficult to distinguish ductility dip cracks from liquation cracks. Both types of cracking appear blunt and intergranular. Confirmation can only be achieved by examining the crack fracture surface. The fracture morphology of ductility dip cracks was found to be generally smooth-intergranular or ductile-intergranular depending on the temperature at which the cracking occurred and the DDC susceptibility. Fracture surfaces at higher temperature or in more susceptible material would be typified by a smooth-intergranular mode. Fracture surfaces at lower temperatures or in more resistant material would be more ductile-intergranular. The ductility dip cracks do not exhibit any liquated surface films and often display thermal striations on the fracture surface, which is indicative of exposure at an elevated temperature⁽⁴⁾. A single crack may transition from smooth-intergranular at high temperature to ductile-intergranular at lower temperatures. At slow strain rates a single crack may transition from a liquation/solidification crack to a solid state ductility dip crack. At low magnification, the lower temperature fracture surface may appear very smooth, however at high magnification, 2000x, the fracture surface exhibits "micro-dimples".

Conclusions:

- 1) The spot-on-spot vareststraint testing technique is an effective test method to produce HAZ DDC and to order rank the material tested relative HAZ DDC susceptibility. The DDC lower temperature bound and the threshold strain provided the greatest insight and consistency.
- 2) The transverse vareststraint test successfully produced fusion zone DDC, but provided limited separation of the test materials due to variable grain boundary orientation with respect to the applied strain
- 3) Of the materials tested, wrought Alloy 600 was the least susceptible to both fusion zone and HAZ DDC. This is attributed to its fine grain size in the wrought condition.
- 4) Alloy 690 and Filler Metal 52 exhibit high DDC susceptibility as compared to the other nickel-based

materials of this study.

- 5) Large straight grain boundaries are particularly susceptible to DDC as demonstrated by the increased DDC susceptibility with the large grains produced by pre-spot weld conditioning.
- 6) Improved DDC resistance occurs with materials with grain boundary precipitates or second phases, which limit grain boundary migration and grain growth as demonstrated in the DDC susceptibility difference between FM 52 and FM 82.
- 7) Rotating a weld deposit 90° relative to the applied strain reduces the apparent grain size of a weld deposit and significantly improves DDC resistance of FM 82.

Acknowledgements:

Special recognition is given to MJ Cola who conducted the initial studies, which set the direction of this work, and to the Edison Welding Institute where the experiments were conducted under Dr. Randy Bowers. The special consultations from Dr. John Lippold were also very instrumental in this work.

References:

- 1) B.B. Hood and W. Lin, 1995, "Weldability Testing of Inconel Filler Metals", Presented at the 7th International Symposium on Environmental Degradation of Materials in Nuclear Power Systems – Water Reactors, August 6-10, 1995, Breckenridge, CO.
- 2) W. Lin and M. Cola, 1997, "Weldability of Inconel Filler Metal 52", Abstracts of Papers, Presented at the 78th Annual AWS Convention, Los Angeles, CA, April 13-17, 1997.
- 3) Dr. Barry M. Patchett, 1995, The Metals Blue Book. Welding Filler Metals, Published by CASTI and AWS, p. 36.
- 4) J. Lippold, M. Tumuluru, and W.A.T Clark, 1992, "An Investigation of Weld Metal Interfaces", The Metal Science of Joining, Published by TMS, Warrendale, PA, pp. 141-146.

Table 1. Nominal Compositions of Test Metals.

Element	Alloy 600	Alloy 690	FM 52	FM 82	FM 625
Ni	76.	59.94	60.49	72.7	64.6
Cr	15.6	30.04	28.97	20.0	21.9
Fe	8.56	9.13	8.86	0.98	0.6
C	.08	0.028	0.022	0.05	0.01
Mn	0.22	0.14	.24	2.91	0.14
S	0.02	0.001	<0.001	0.004	0.003
Si	0.24	0.08	.14	0.10	0.07
Mo	0.18	0.037	0.003	--	8.8
Nb	0.07	0.006	0.01	2.6	3.55
P	0.009	0.005	0.004	0.003	0.01
Al	0.25	0.19	0.69	--	0.21
Ti	0.30	0.29	0.58	0.31	0.25
Mg	0.022	<0.008	0.015	--	--

Table 2. Vareststraint Test Parameters

Transverse		Spot-on-Spot		
			Pre Spot	Test Spot
Current	180 amps	Current	200 amps	150 amps
Travel	6 ipm	Voltage	13 volts	12 volts
Arc Gap, inch	0.09375	Downslope to current	50 amps	N/A
Voltage	11-13 volts	Ramp Time	10 sec	N/A
Weld Length at Bending, inches	1.25	Hold Time	20	5 sec
Total Weld Length	1.5	Downslope Time	10 sec	
Gas Shielding	Argon	Delay Time	N/A	0.5 sec
Bend Rate	10 ips	Bend Rate	N/A	10 ips
		Gas Shielding	Argon	Argon

Table 3. Results of the Transverse Varestraint – Each Test Result is the Average of Three Tests.

Test Material	Augmented Strain, %	No. of Cracks	Total Crack Length, mm	Crack Location, mm	No. of Cracked Specimens	Cracking Temperature Range, C	Threshold Strain Rate, ips	Threshold Strain, %
FM 52	7	4.33	3.07	3.4-11.6	3	1162-908	0.05	<4
	5	1.67	1.98	3.3-8.9	2	1167-965		
	4	0.33	0.17	9.4-10.0	1	952-941		
FM 82	7	4.33	3.35	3.1-11.4	3	1190-918	0.05	<4
	5	1.33	0.42	4.1-5.1	1	1139-1092		
	4	0.33	0.08	2.9-3.1	1	1207-1190		
FM 625	7	0.67	0.71	3.5-8.0	2	1175-990	2.0	5
	5	0.33	0.12	4.5-4.9	1	1123-1100		
	4	0	0	0	0	--		
Alloy 690	7	7.33	3.12	2.7-10.3	3	1200-935	0.04	<4
	5	2.3	1.53	6.5-11.2	3	1032-916		
	4	1.67	0.39	1.9-8.1	2	1252-985		
Alloy 600	7	0	0	0	0	--	>10	>7

Table 4. Results of Spot and Spot-on-Spot Varestraint, * average of three tests.

Test Material	Augmented Strain, %	Number of Cracks	Cracking Location, mm	Cracking Temperature Range, C	Threshold Strain, %	Width of Temperature Range, C
FM 52, Pre-Spot	10	9	+1 to -1.5	895-1255	2	360
	7	7	+1.38 to -1.0	840-1185		325
	5	3	+0.25 to -1.5	1005-1255		250
FM 82, No Pre-spot*	10	6.7	-0.33 to -1.9	1065-1308	3	243
	7	5.7	-0.39 to -2.04	1073-1320		247
	5	2.7	-1.14 to -1.92	1185-1302		117
FM 82, Pre-Spot*	10	11.3	+1.87 to -1.92	987-1308	2	321
	7	10	+0.14 to -2.05	993-1300		307
	5	5.7	-0.64 to -1.65	1110-1260		150
FM 82, 90 Orient.	10	15	0 to -2.0	1015-1315	Not Performed	300
	7	11	+0.15 to -2.0	995-1315		320
	5	6	-0.13 to -1.88	1035-1295		260
FM 625, Pre-Spot	10	Some DDC identified but extensive liquation cracking prevailed				
	7					
	5					
Alloy 600, No Pre-Spot	10	1	-1.23 to -1.5	1200-1240	10	40
	7	0	--	--		--
	5	0	--	--		--
Alloy 600, Pre-Spot	10	7	+0.25 to -2.0	980-1315	3	335
	7	6	0 to -1.75	1015-1280		265
	5	6	0 to -1.8	1015-1280		270
Alloy 690, No Pre-Spot	10	11	0 to -0.23	1000-1330	3	330
	7	7	+0.53 to -2.05	1080-1320		240
	5	4	-0.8 to -1.85	1125-1290		165
Alloy 690, Pre-Spot	10	12	0 to -2.35	875-1310	1	435
	7	3	+0.5 to -1.79	900-1265		365
	5	6	+0.025 to -1.2	960-1185		225

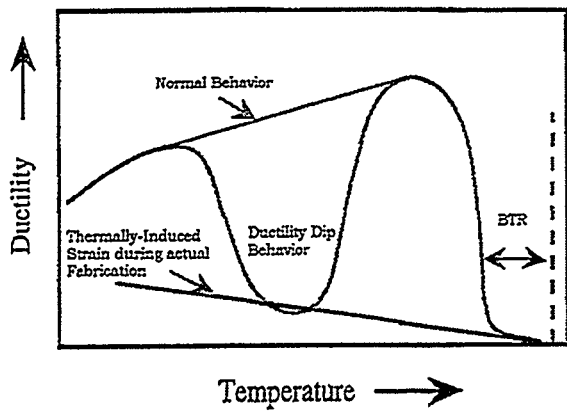


Figure 1. Illustration of Ductility Dip Behavior with Temperature. (BTR, Brittle Temperature Range)

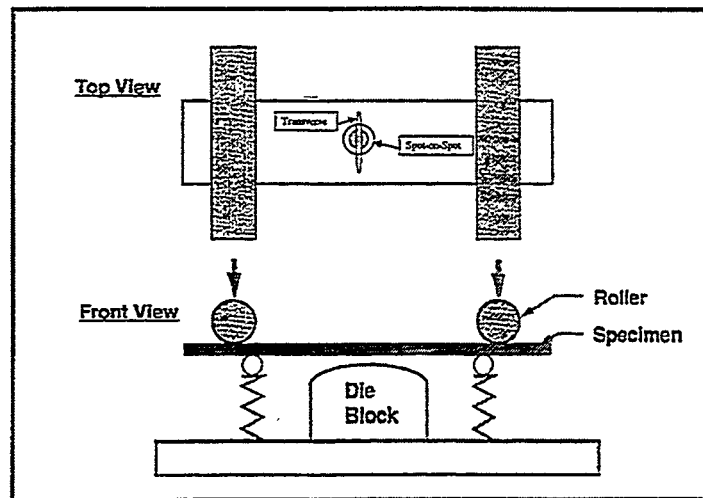


Figure 2. Schematic of the Universal Varestraint Testing For Transverse and Spot-on-Spot Testing.

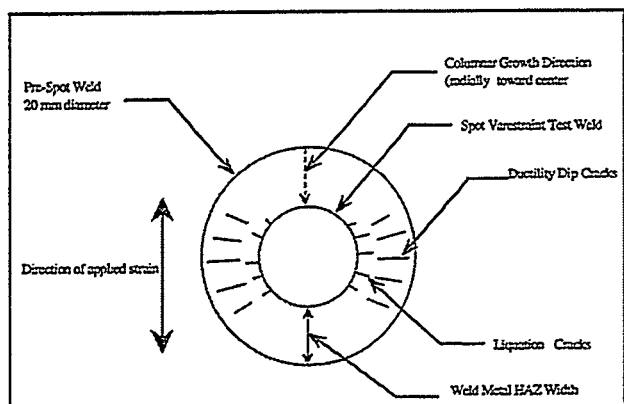


Figure 3. Illustration of the Spot-on-Spot Varestraint Test for Weld Metal HAZ Ductility Dip Cracking.

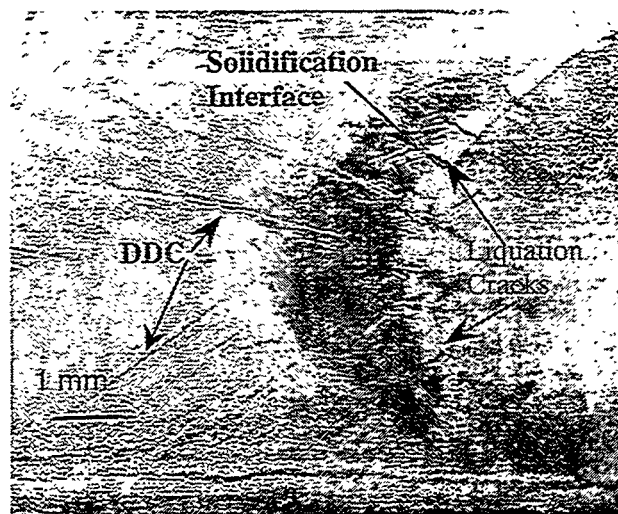


Figure 4. Transverse Varestraint Test Weld, FM 52, 7% Augmented Strain, 10 ips.

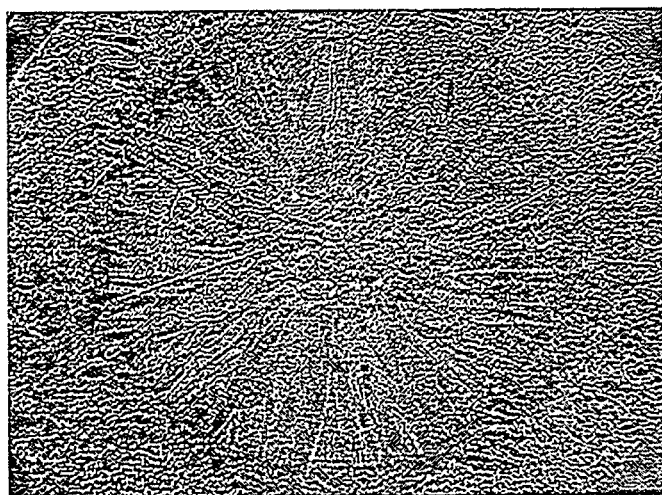


Figure 5. Plan View Micrograph of Pre-Spot on FM 52 Transverse Varestraint.

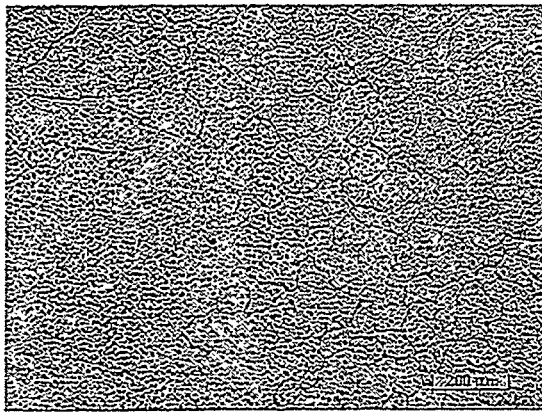


Figure 6a. Initial Microstructure of FM 52 Weld Deposit.



Figure 6 b. Pre-Spot Microstructure of FM 52.

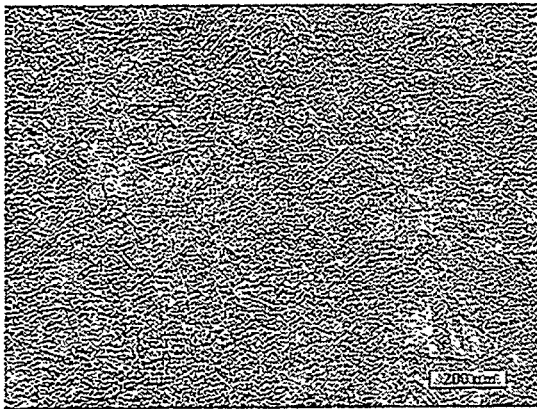


Figure 7a. Microstructure of Wrought A600.

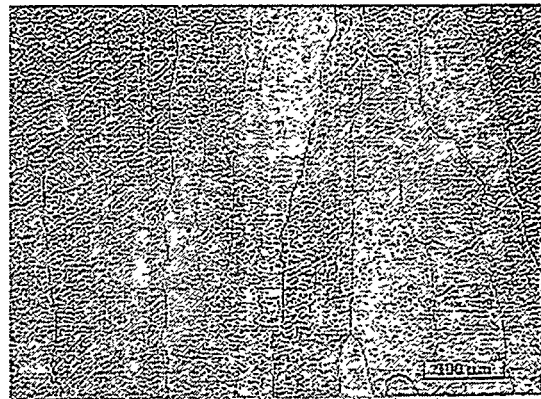


Figure 7 b. Pre-Spot Microstructure of A600.

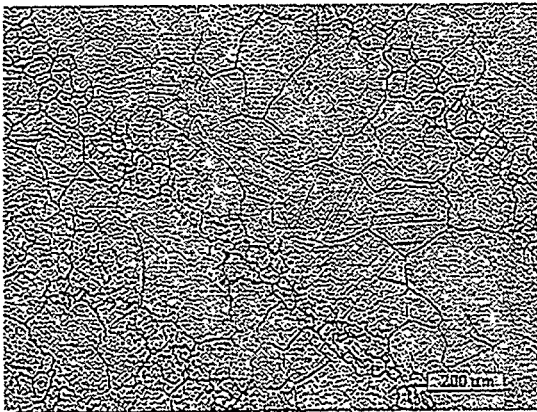


Figure 7c. Microstructure of Wrought A690.

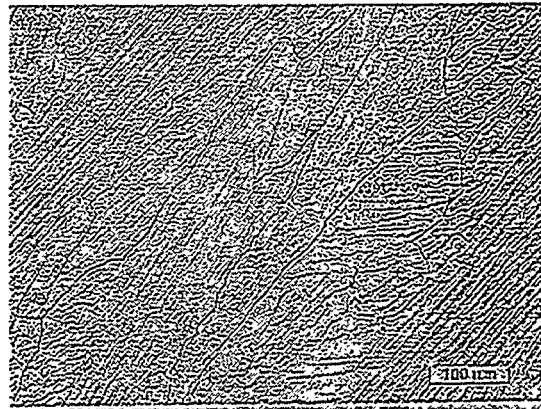


Figure 7d. Pre-Spot Microstructure of A690.

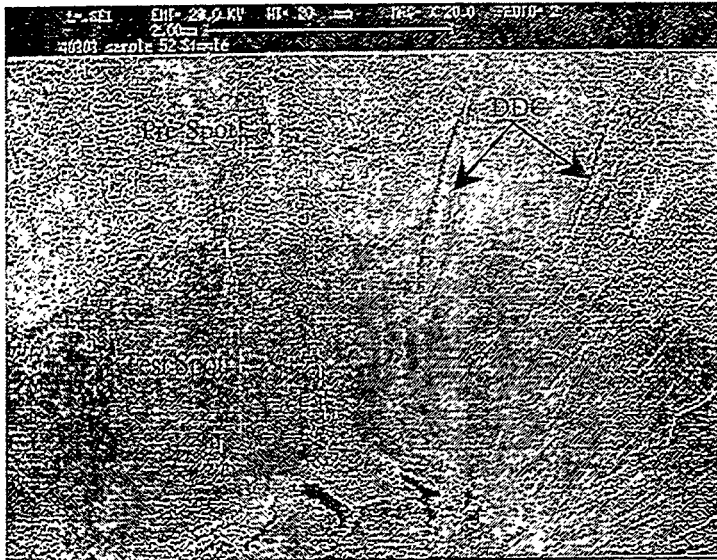


Figure 8. Spot-on-Spot Varestraint Test Weld, FM 52, 10% Augmented Strain, 10 ips.

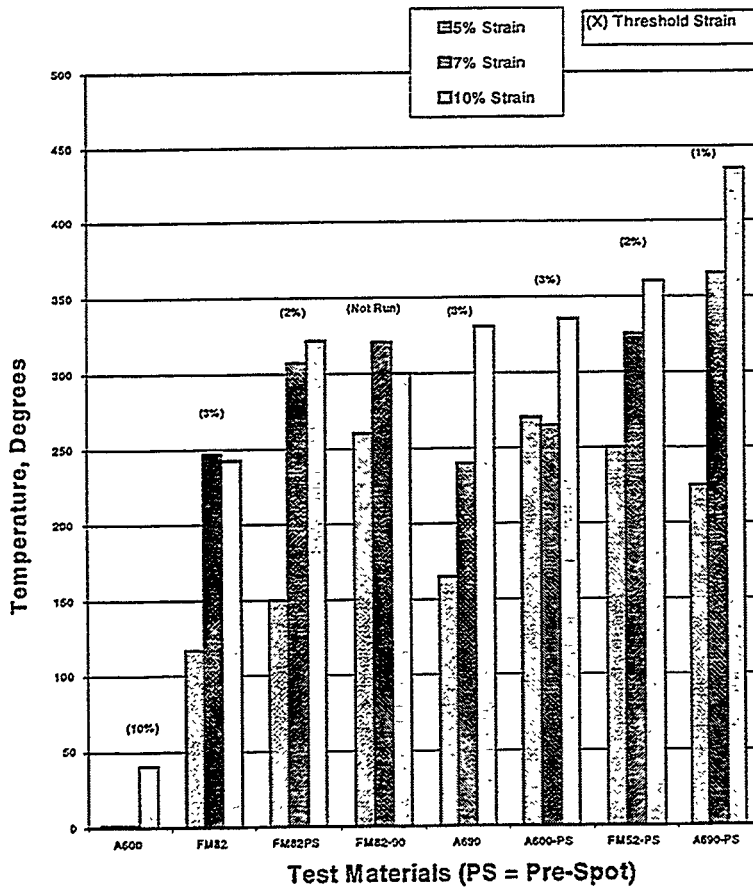


Figure 9. DDC Temperature Range from Cracking Locations in Spot-on-Spot Varestraint Tests.

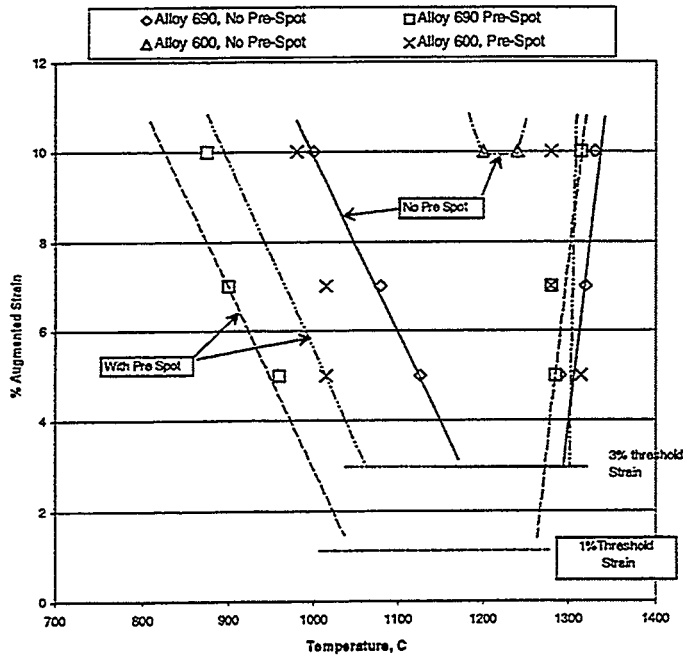


Figure 10. Ductility Dip Envelope for Alloy 600 and Alloy 690 from Single and Spot-on-Spot Vastrestraint Tests.

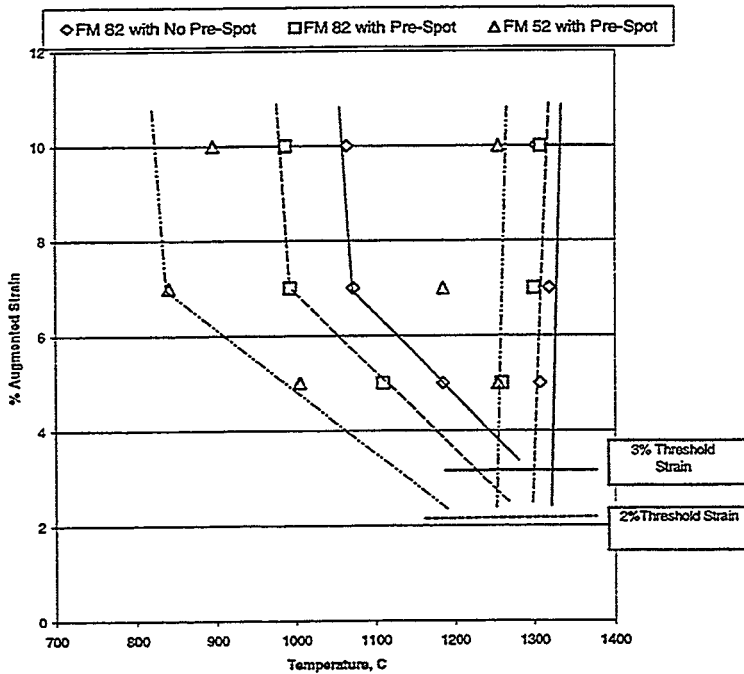


Figure 11. Ductility Dip Envelope for FM 82 and FM 52 from Single Spot and Spot-on-Spot Vastrestraint Tests. Each FM 82 point, with and without a pre-spot, is the average of three tests.

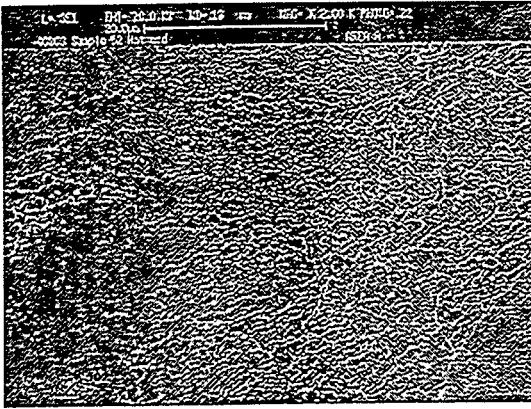


Figure 12a. Fractograph at High Temperature End of Ductility Dip Crack in FM 52 Spot-on-Spot Sample.

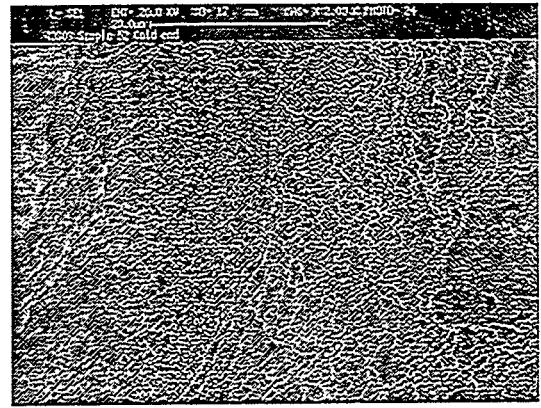


Figure 12b. Fractograph at Low Temperature End of Ductility Dip Crack in FM 52 Spot-on-Spot Sample.

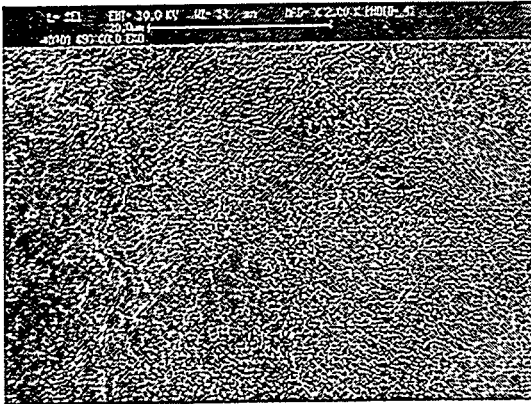


Figure 13a. Fractograph at High Temperature End of Ductility Dip Crack in Alloy 690 Spot-on-Spot Sample.

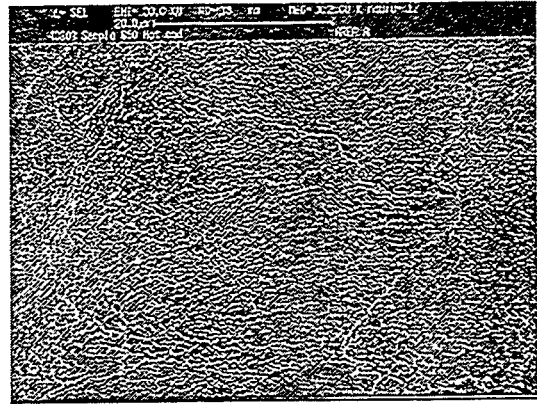


Figure 13b. Fractograph at Low Temperature End of Ductility Dip Crack in Alloy 690 Spot-on-Spot Sample.

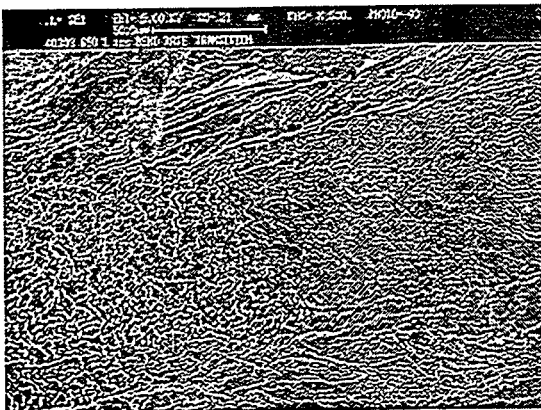


Figure 14. Fractograph at Transition Region to Ductility Dip Cracking in Alloy 690 Spot-on-Spot Vastrestraint Test at 1 inch per second Bend Rate, 7% Strain, 0 second Delay Time.